Morphology, Particle Size Distribution, and Composition in One- and Two-Salt Metal Oxinate Liesegang Patterns

Lara Mandalian,[†] Mazen Fahs,[†] Mazen Al-Ghoul,[†,‡] and Rabih Sultan*[,†]

Department of Chemistry and Center for Advanced Mathematical Sciences, American University of Beirut, Beirut, Lebanon

Received: May 22, 2003; In Final Form: November 6, 2003

Precipitate systems consist of particles of various sizes distributed in space. The determination of the particle size distribution (PSD) in a precipitate allows a better understanding of the spatio-temporal dynamics of such a system. The Liesegang method of growing precipitates in gels slows down the kinetics of precipitation to a diffusion-controlled limit and yields exotic patterns of parallel salt bands. This promotes the possibility of measuring the PSD, especially when bands with well-dispersed particles in space are obtained. Such an experiment was realized in our laboratory on cobalt(II) oxinate yielding appropriate patterns with exactly the desired features. We here attempt to improve and quantify these experiments, to measure the PSD using different analysis methods. The measurements are performed via two routes: in the laboratory under the microscope and by image analysis of 2D pictures of the various bands. The two methods show a good qualitative agreement in that the trends are almost perfectly reproduced. The band morphology is studied notably as a function of initial supersaturation, and novel features related to particle size and number density are observed. Two-salt metal oxinate patterns are prepared and analyzed.

1. Introduction

Periodic precipitation takes place when two coprecipitate ions interdiffuse in a gel medium. When the experiment is carried out in a tube, the sparingly soluble salt may precipitate out in forming a beautiful set of parallel bands. This phenomenon, discovered in 1896, is known as Liesegang[1] banding. It still attracts interest[2] because of its potential applications and similarities with natural pattern forming systems in biology[3−6] and geology[7−10] on one hand and its rich nonequilibrium dynamics involving the coupling of diffusion and precipitation chemical reactions on the other hand.

A precipitate is a large collection of small particles of different sizes which exhibits a dynamic evolution, until the system reaches thermodynamic equilibrium. The sizes of particles initially born obey a spatial distribution which can be expressed mathematically in different forms, such as a random noise distribution[11] or a small amplitude disturbance in a localized spatial position.[12−14] Because of surface tension effects, the smaller particles have a higher solubility than larger particles; the coupling of this effect to the diffusion of the dissolved ions results in larger particles growing at the expense of smaller ones. Consequently, the system evolves with time toward a state of fewer but larger particles. This interesting phenomenon resulting from the competitive growth of precipitate particles[12] is traditionally known as Ostwald ripening.[15,16] The modeling of the competition between particle ensembles was initiated in a pioneering paper by Lifshitz and Slyosov.[17]

Liesegang experiments involving organic and organometallic materials have been considered but remain relatively scarcely explored. Compounds involving complex formation, notably metal-chelate precipitate systems,[18] may exhibit interesting patterning properties. More than one nucleation outburst,[18] and in Liesegang banding, revert spacing under certain conditions,[19] have been reported. Precipitate patterning experiments recently performed in our laboratory[20] involved the precipitation of cobalt(II) oxinate as suggested by Kanniah et al.[21] The oxinate ligand (from oxine ≡ 8-hydroxy-quinoline) and the square planar Co(II) oxinate complex[22] are shown in Figure 1. The present paper studies various aspects of this pattern formation, spanning the morphology of the bands, the patterning schemes in two-precipitate systems, and mainly the particle size distribution (PSD) and its variation with initial supersaturation and the time evolution of the pattern.

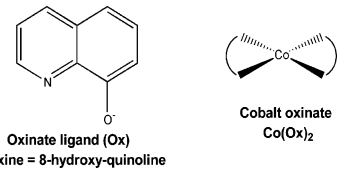

Figure 1. The oxinate ligand and the cobalt(II) oxinate complex.

The aims of the present paper are outlined as follows:

a. Performing experiments on cobalt(II) oxinate Liesegang patterns, yielding band zones of precipitate that are either compact or consisting of a scatter of spots, depending on the conditions.

b. Analyzing the band zones in the tube under the microscope to obtain the PSD expressed as the spatio-temporal variation of the number of bands and the average particle diameter (taking the particles to be small spheres).

c. Developing an image analysis method for the simulation of the PSD by analyzing scanned two-dimensional pictures of the individual spotted bands. The results of this method will be compared with those of the true laboratory analysis. If the results are in good agreement, this method could be a powerful alternative to the tedious operation of pulling the gel out of the

* Address correspondence to this author. E-mail: rsultan@aub.edu.lb.
† Department of Chemistry.
‡ Center for Advanced Mathematical Sciences.

10.1021/jp035421s CCC: $27.50
Published on Web 01/06/2004

tube, its "dissection" band by band, and the subsequent collection of all the particles for a number count and a measurement of size.

d. Performing experiments wherein two salts are precipitated (such as the oxinates of Co and Cu on one hand and those of Co and Zn on the other) and then analyzing the different patterns obtained.

e. Comparing the results with other studies on precipitate pattern formation and coarsening found in the literature.

2. Experimental Section

2.1. Cobalt Oxinate Liesegang Patterns. The procedure is a variant of that described previously.[21,20] 0.218 grams of 8-hydroxy-quinoline (oxine, Merck) are dissolved in 2.0 M acetic acid, and the solution is well stirred for about 5 minutes. Then, 25% ammonia solution is added drop by drop with constant stirring until a faint but permanent turbidity is obtained. This turbidity is redissolved by adding a few more drops of acetic acid (2.0 M), and then the solution is stirred vigorously until it becomes totally clear. The pH of the solution is measured at this point and is between 4.0 and 4.1 (above the threshold for the precipitation of cobalt oxinate[23]). The mixture is made up to 50.0 mL with double-distilled water, yielding a 0.030 M oxine solution. To this solution, 0.505 g of agar (Difco) is added, and the mixture is heated to 90 °C and stirred for 10−15 min until a clear solution is obtained. The latter is poured while hot into thin tubes of length 30.0 cm and inner diameter 6.0 mm, which are then allowed to cool and stand overnight for gelation. The next day, a few milliliters of a 0.515 M $CoCl_2$ solution (prepared from $CoCl_2 \cdot 6H_2O$, Fluka) is added on top of the solidified gel. Brown bands of cobalt oxinate start appearing within 10−12 h.

2.2. Two-Salt Systems and Their Analysis. The same procedure for the preparation of the gel-oxine medium in the tube is followed here (0.0100 M oxine is used). However, the solution delivered on the top contains two metal ions: Co^{2+} (0.0759 M) and Cu^{2+} (0.100 M) in one case, and Co^{2+} (0.0759 M) and Zn^{2+} (0.150 M) in the other. Different types of patterns are obtained (see Section 4) which are analyzed for their distribution in the various precipitates. A given tube containing a two-precipitate pattern is cut at its bottom edge and the gel is allowed to slide on a tall glass plate. Each band (precipitate-containing gel portion, of compact appearance or consisting of a scatter of visible particles) is cut and is placed in a centrifuge tube. Water is added to the tube, and the mixture is heated to liquefy the gel and then centrifuged and filtered while hot. The precipitate particles retained by the filter paper are washed thoroughly and left for complete drying. Alternatively, the gel could be dissolved in DMSO[24] and the solution filtered, leaving the undissolved salt particles on the filter paper. Both methods were tried, but the centrifugation method gave better results.

The dry crystals of a given band are weighed by difference (crystals with filter paper, then filter paper alone) and transferred to a small beaker. They are then dissolved in 2−3 mL of 6 M nitric acid. The resulting solution is analyzed for metal-ion content (Co^{2+}/Cu^{2+} or Co^{2+}/Zn^{2+}) using atomic absorption spectrophotometry.

3. Band Morphology

In addition to the classical Liesegang patterns[21] with coarse bands, we obtained Co(II) oxinate patterns with periodic precipitate zones consisting of dispersed particles, easily distinguishable with the naked eye, as shown in Figure 2. We mainly distinguish between three levels of particle distributions,

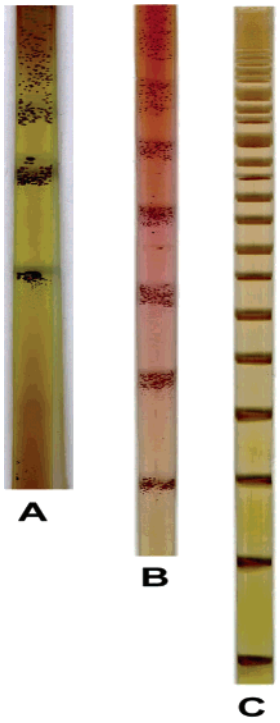

Figure 2. Tubes of cobalt oxinate Liesegang patterns with different textures: A (dense, age 84 days), B (scattered, age 185 days), and C (compact, age 161 days).

in three corresponding textures that we call compact (C), scattered (B), and dense (A). In the compact structure (C), the bands appear as homogeneous zones wherein individual particles are not discernible with the naked eye. A scattered distribution refers to bands constituted of fine particles that are spread over a relatively broad stripe (B). The dense type of band (A) consists of particles that are large to an extent leaving very little space between them (nearly touching neighboring spheres). Every tube was prepared in triplicate, and a good reproducibility was obtained. It is useful here to recall two parameters, Δ and σ (initial concentration difference and initial supersaturation, respectively), introduced by Müller et al.[25] and defined as follows:

$$\Delta = \left|\frac{1}{2}[\mathrm{Ox}]_o - [\mathrm{Co}^{2+}]_o\right| \quad (1)$$

$$\sigma = [\mathrm{Co}^{2+}]_o[\mathrm{Ox}]_o^{\,2} \quad (2)$$

where "Ox" denotes the oxinate ion and the subscripts "$_o$" indicate the initial concentrations used. The parameters Δ and σ were shown[25] to play a key role in determining the band morphology in Liesegang patterns. In the present study, we notice that we can go from one texture to the other by mainly varying the suspersaturation parameter, σ, at constant Δ (see Table 1). Experiments were also performed while varying Δ at constant σ. Over the explored range, this also resulted in changing the texture of the bands, but to a much lesser extent.

The last band of each of the patterns A, B, and C is observed under microscope, and an enlarged representative portion (a frame of length 2.25 mm and width 1.70 mm) is photographed. The average particle size in each tube is measured by an image analysis technique described in Section 4.2. A typical trend of particle size variation (decrease) from tube A through C is displayed in the photomicrographs of Figure 3. The measurements are reported in Table 1. We see that as σ is increased (at

TABLE 1: Conditions for Obtaining Different Types of Cobalt Oxinate Patterns: Initial Concentrations, Concentration Differences (Δ), and Supersaturations (σ)[a]

tube	$[Co^{2+}]_o$	$[Ox]_o$	$\Delta \times 10^3$ (M)	$\sigma \times 10^6$ (M^3)	pattern type	av diameter $\bar{d}$ (mm)	no. of bands
1	0.112	0.0829	70.6	769	A	0.59	3
2	0.0859	0.030	70.9	77.3	B	0.38	7
3	0.0759	0.0101	70.9	7.74	C	0.045	24

[a] For each type of pattern obtained (A, B, or C), the number of bands and the average particle diameter ($\bar{d}$) are reported.

constant Δ), the number of bands decreases, while the average particle size of the grains constituting the last band increases. Figure 3 also reveals that the particle number density within a given band decreases with increasing initial supersaturation. The latter quantity was not measured in this case because the image analysis method yields only a 2D number density. Müller et al.[26] reported a dependence of the PSD on initial supersaturation by analyzing a 2D supercooled PbI_2 pattern from a hot homogeneous solution of the salt. However, they found a trend exactly opposite to the one observed in our study. Their system differs from ours in three main aspects: (1) their experiment is carried out in the absence of any concentration gradient; (2) the aging time is relatively short: one week compared with 12−26 weeks in our experiments; and (3) in our system, the anion is a chelating ligand. The level of supersaturation governs the rates of particle nucleation and growth and thus influences the resultant particle size and its distribution, as well as the particle morphology.[27] The equilibrium particle size distribution is thus a result of the interplay between the rate of nucleation and that of particle growth.[28,29] Although particle size seems to generally decrease with increasing relative supersaturation,[29−31] the opposite behavior has been observed in some systems.[32−35] Higher nucleation rates favor the production of a larger number of particles.[29,34] Because we obtain fewer but larger particles (Table 1 and Figure 3) at higher supersaturation, it appears that we are in a regime where the rate of particle growth dominates over that of nucleation. This may be attributed to the more complex precipitation scheme in this ion-chelate precipitation and the nonhomogeneous spatial precipitate distribution in the presence of the gradient. Our system thus presents an interesting situation, which warrants further investigation. Finally, the last column in Table 1 shows the number of bands in each system after the tubes have aged for different times (see the caption of Figure 2). In all tubes, no new bands were formed after some time had elapsed, beyond which the number of bands remained constant.

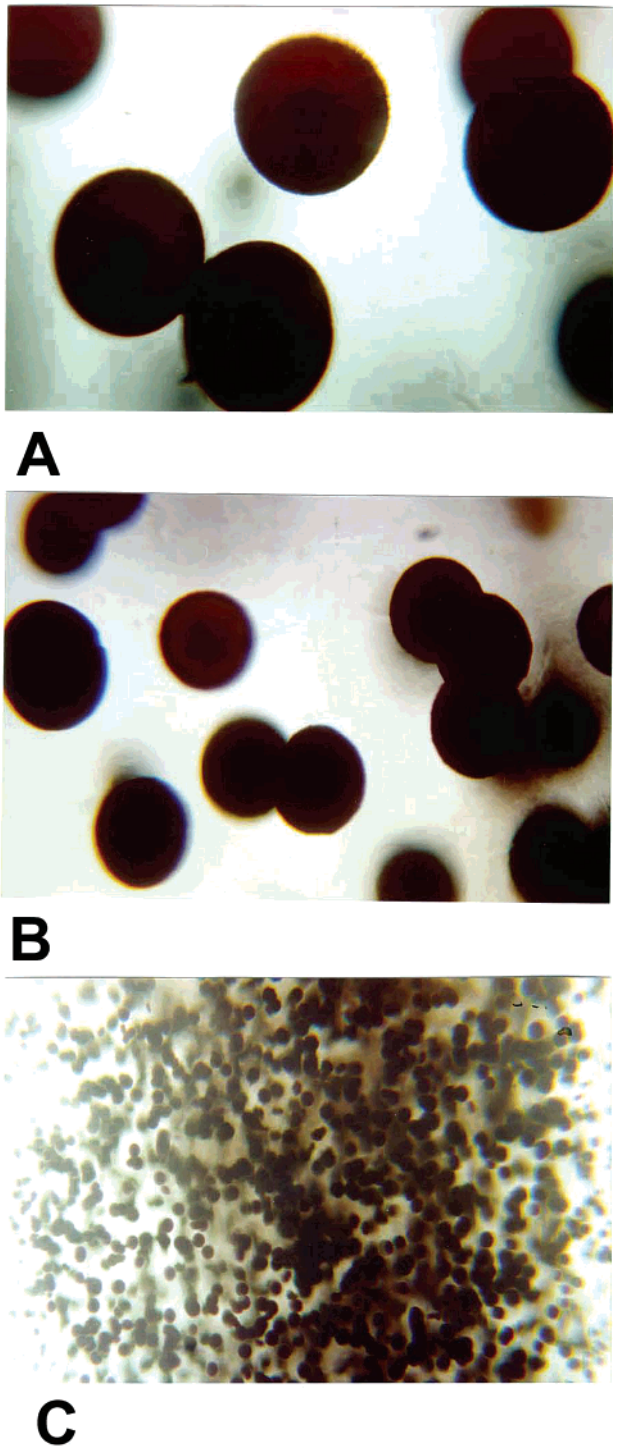

Figure 3. Bands of tubes A, B, and C under the microscope. The number of particles decreases and the average particle size increases with initial supersaturation σ (i.e., as we go from C to B to A; see Table 1 for numerical values).

4. Pattern Evolution

By examining the various bands of granular type in a given pattern (in the same tube, here), we remarked that the average particle size is not uniform in all of them, but increases with band number, that is, as we go down the tube. We further noticed that the number of particles decreases as we go from top to bottom, that is, the bands at the bottom contain considerably less particles of larger size than the ones at the top. It is believed that those two observations are dominated by an aging mechanism of the Ostwald ripening type (see Section 1).

4.1. Ostwald Ripening Probes. Early experimental work on the verification of Ostwald ripening was previously based on studying the coarsening of precipitate zones, probed by a measurement of the length scale of the patterns.[12,19,26,36] The latter was described by the size of pores separating dense precipitate regions, in 1D[19,36] and 2D[12,26] mosaic PbI_2 patterns. Microscope pictures[26] enabled the measurement of the number of particles and their sizes within a dense domain. Optical methods[37] (such as measurements of transmitted light, scattered light, and refractive index) were used for the determination of particle number density in $Mg(OH)_2$ and PbI_2 Liesegang patterns. Electron transmission microscopy is an elaborate technique for identifying the microstructure of alloys subjected to annealing treatments[38] and liquid phase sintered hard metals.

Our approach resides in directly determining the particle size distribution over the various bands of a cobalt oxinate Liesegang pattern.

Though the Liesegang banding phenomenon dates back to the 19th century, debate still exists as to its origin and mechanism. Theories of periodic precipitation generally fall into either one of two broad categories: pre-nucleation theories based on the Ostwald−Prager (OP)[39,40] supersaturation-nucleation-depletion cycle and post-nucleation theories developed by Ross,[14,37] Ortoleva,[12,13] and their co-workers on the basis of the competitive growth of the particles (CPG theory). Growth kinetics was modeled via the Becker−Döring stepwise aggregation and fragmentation equations.[41,42] Recently, Ozkan and Ortoleva[43] developed an algorithm for calculating the dynamics of the particle size distribution (PSD), on the basis of unit cell addition cascade of the form:

$$aX + bY + S_n \rightleftharpoons S_{n+1} \tag{3}$$

where a and b are stoichiometric coefficients and S_n is a cluster of n formula units X_aY_b. Such a chemical kinetic formulation bridges the transition from monomer and dimer to macroparticle (10^{23}-mer). Application of the model to the silica polymorph system revealed a growth of the average radius with time t with a proportionality to $t^{1/2}$. A comprehensive review of mathematical techniques for the treatment of coarsening is presented in ref 16.

4.2. Laboratory Analysis. The bands in the various patterns (see Section 3) range from a dense texture to a scatter of spots, and thus span the microscopic, mesoscopic, and macroscopic length scales. We select a typical pattern of macroscopic texture (type B) for the analysis of the PSD (concentrations: $[Ox]_o = 0.0300$ M, $[Co^{2+}]_o = 0.515$ M, [agar] = 10 mg/mL; parameters: $\Delta = 0.500$ M, $\sigma = 4.64 \times 10^{-4}$ M). The tube was allowed to age for a long time (3.6 years). The bands were numbered in increasing order from top to bottom, as shown in Figure 4. The gel was extracted smoothly from the tube as was done in the two-salt band analysis (described in Section 2.2). Each band was cut at its edges and placed in a small vial. The bands were then analyzed one by one under the microscope as follows: a gel portion containing the grains of a given band was spread under the microscope, and a count of the particles was performed. The diameter of each particle was then measured by means of a minute, 1.00 mm scale reticle. The average particle diameter ($\bar{d}$) was calculated for each band. Figure 5 shows a plot of the variation of the number of particles (N, frame a) and the average particle diameter ($\bar{d}$, frame **b**) with band number. We clearly see that the dominant trend is a decrease in the number of particles and an increase in the average particle size with increasing band number. A histogram representation of the PSD over the five last bands in the pattern with best Gaussian fits (adopted from Kai et al.[44]) is seen in Figure 6. This result reveals a new route for the quantitative verification of Ostwald ripening, within the dynamics of the whole system. It is well known[16] that the processes of nucleation, growth, and coarsening do not generally occur in a strict sequence but overlap. We believe that coarsening (as described in Section 4.1) plays a dominant role in the observed spatio-temporal evolution of the pattern. The same trend was observed within the domain of one same band, that is, the evolution of the latter toward a state of fewer but larger particles. However, this has not been monitored via a quantitative measurement. On the basis of a purely prenucleation model where no ripening is considered, Dee[45] obtained indeed a decreasing number density with distance in the treatment of a Liesegang problem.

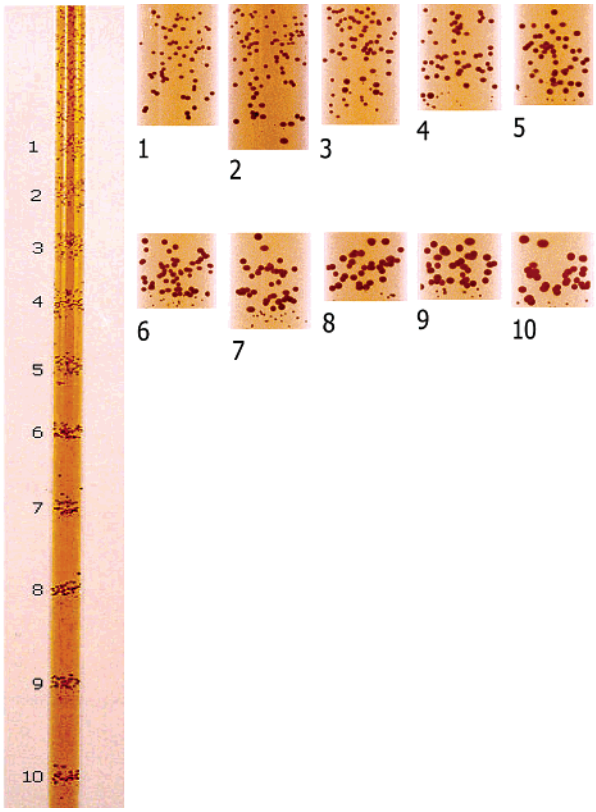

Figure 4. Ostwald ripening in an aged tube (3.6 years). (a) Whole tube with bands numbered 1−10. (b) Enlarged pictures of the individual bands. $[Ox]_o = 0.0300$ M, $[Co^{2+}]_o = 0.515$ M, [agar] = 10 mg/mL. The pattern coarsens with increasing band number.

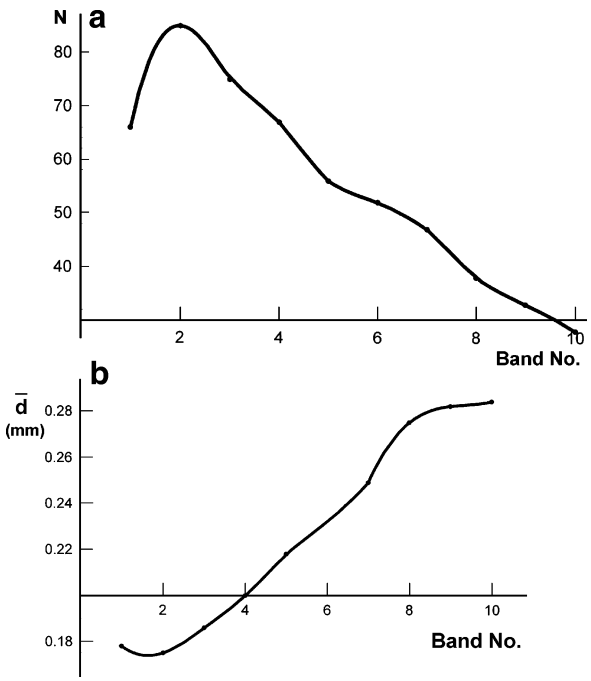

Figure 5. (a) Plot of number of particles N (within a given band) versus band number. (b) Plot of average particle diameter ($\bar{d}$) versus band number. The measurements are performed on the tube in Figure 4 by a laboratory analysis described in Section 4.2.

However, the quantity appears to reach a constant value in a nearly asymptotic form. The decrease is not as sharp over the last bands as is observed here. No plot of the particle radius versus distance was displayed in the paper. In the present study,

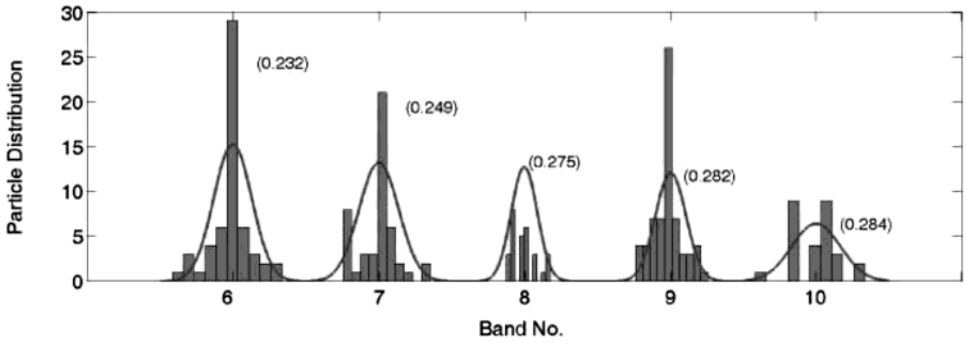

Figure 6. Particle size distribution (PSD) for the last five bands (6−10) in the tube of Figure 4a, shown as histograms with best Gaussian fits. The Gaussian curves are standardized by multiplying the ordinate by the total number of particles in a particular band and dividing by the number of particles in band 6. The numbers indicate the average particle diameter (mm) for a given band.

we have allowed the tube to age for an unusually long time (3.6 years). The sharp trend we obtain here could not have possibly been arrived at without such aging. This realization seems to support an important role of the ripening process in the overall observed dynamics.

4.3. Image Analysis. In this section, we describe the numerical method used to automatically count the number of particles within a given band and measure the average particle diameter. The method is derived from digital image analysis which is extensively used and widely applied in numerous areas. A two-dimensional image of the three-dimensional band domain is taken (Figure 4b) and then processed using a series of codes written in C and Matlab. Hence, the particles which are spherically shaped become overlapping circles when the two-dimensional picture is considered. The main difficulty in counting the number of particles lies in the aforementioned overlap of resulting circular shapes. Let us define some terminology that we are going to use repeatedly in this section. A blob designates a set of connected circular shapes. These welded circles will be called the bubbles of the blob. A blob may be formed by only one bubble. If a blob contains more than one bubble, then a suitable algorithm is required to resolve overlapped bubbles into individual ones.

We first started using a counting algorithm based on the Hough transform.[46] This yielded inaccurate counting as expected for two main reasons. First, many shapes present in the analyzed image are not real circles. Second, the overlap in many blobs frequently exceeds 30% which makes it very difficult for the Hough transform to resolve such an overlap. We then decided to count bubbles by counting the cusps or the sharp variations in the detected edge of the blobs. This method also yielded a bad count. We finally resorted to the watershed segmentation method[47,48] which proved to be much more successful.

The term watershed refers to a ridge that divides areas drained by different river systems. A catchment basin is the geographical area draining into a river or reservoir. The watershed segmentation method is based on the distance transform of a binary image, which is a pixel-to-pixel transform that associates every pixel to the distance from this pixel to the nearest nonzero-valued pixel.

Let us consider an image $\mathscr{I}_n$ of the nth band to be analyzed. This image is initially in RGB format. The first operation on $\mathscr{I}_n$ is to convert it to gray scale. The image is then thresholded and opened (an erosion followed by a dilation) by a small disk to get rid of the very small particles and to smooth the borders of the blobs.[48−50] To separate different bubbles in the different blobs in image $\mathscr{I}_n$, we first compute the distance transform of the complement of $\mathscr{I}_n$, $\mathscr{I}_n^c$. To turn the bright areas into catchment basins, we need to negate image $\mathscr{I}_n^c$. In this new image, there is one catchment basin for each object. We then apply the watershed transform on it to get the image $\mathscr{W}$. $\mathscr{W}$ is also called the label matrix, and it contains positive integers corresponding to the locations of each catchment basin. The zero-valued elements of $\mathscr{W}$ are located along the watershed lines, and they are used to separate the objects in the original image.

Ten two-dimensional images corresponding to the 10 different bands of Figure 4 are analyzed using the aforementioned algorithm. In Figure 7a, the dashed curve represents the manual counting of the number of particles in the gel. The solid curve represents the automatic counting done by our program. The correlation between the two curves is excellent and the nearly constant difference between them is because in image analysis, we are counting a two-dimensional projection of the three-dimensional band domain; therefore, much information including the number of particles is lost because of this reduction in dimension. We can also infer from this difference that the particles are homogeneously distributed in space. However, we account for the discrepancy in the count of particles in the ninth band by the fact that the watershed algorithm cannot resolve very closely overlapping bubbles and blobs.

After counting the number of particles in each band, the average diameter of the bubbles is also computed and compared with the manually measured average diameter. The average diameter of the bubbles was deduced from their average surface. This surface was computed by averaging the convex surface of the previously counted bubbles. The convex surface of a given blob is the surface of the smallest convex polygon that can contain this blob. We approximated this convex surface with a circle. In Figure 7b, the comparison between the average diameter measured under the microscope (dashed curve) and that computed by image analysis (solid curve) is depicted. A good qualitative agreement is noted.

5. Two-Salt Systems

The analysis of the two-salt patterns described in Section 2.2 will now be presented. The cobalt oxinate/copper oxinate pattern is shown in Figure 8; the initial concentrations of the reagents are given in Section 2.2 and in the captions of Figure 8 and Table 2. Each band consists of three zones: one dark, dense zone (labeled b) sandwiched between two light, scattered ones (labeled a and c). Photomicrographs of these three domains are depicted in Figure 9. The crystal size in zones a and c (formed at a later stage) is relatively larger and the number density is smaller than in zone b. This seems to be consistent with a ripening mechanism. A similar zonation is observed in rocks[28] and conjectured[28,51] in single-salt precipitate patterning systems.

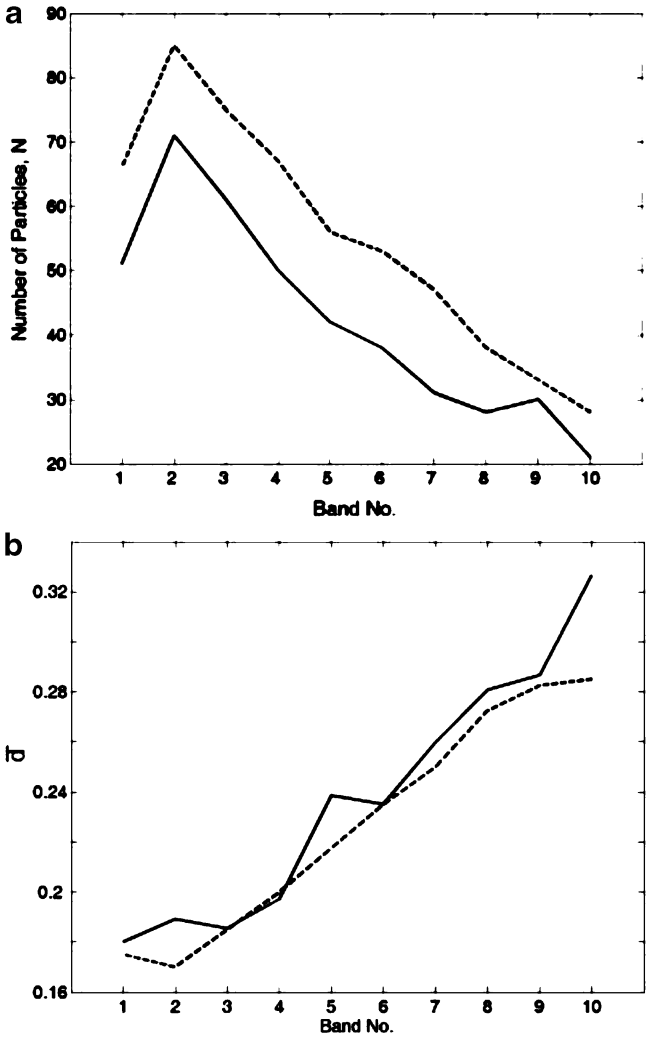

Figure 7. Plot of number of particles (a) and average particle diameter (b) (within a given band) versus band number for the tube of Figure 4, but obtained here from an image analysis technique described in Section 4.3. In both frames, solid line: computed; dashed line: experimental. The results are in good qualitative agreement with those of the laboratory analysis (Figure 5).

A single band was shown to evolve into a "doublet", actually representing a three-zone topology (because of the presence of the minimum in particle radius), just as is observed in our two-salt experiment. While such a band splitting (often referred to as secondary banding[13]) was demonstrated using a ripening and crystal aging mechanism in the work by Feeney et al.[13] and Boudreau,[28] it was also mostly favored under conditions where ripening becomes important in models which include nucleation, growth, and ripening (Chacron and L'Heureux[51]). We recently obtained[52] a band splitting in the simulation of a two-precipitate Liesegang system involving redissolution due to complex formation (the band of each salt exhibited a splitting). Finally, one interesting variant in our observed zoning is that the middle region is more dense in precipitate than the edge zones, just opposing the common observation.

The contents of the various parts were analyzed by atomic absorption spectrophotometry. The Co^{2+}/Cu^{2+} proportions of a given part were converted to relative masses of cobalt oxinate and copper oxinate precipitates. The mass percents are reported in Table 2.

We notice that we almost have a trend of alternating composition in the two salts as we go down from one zone to the next one.

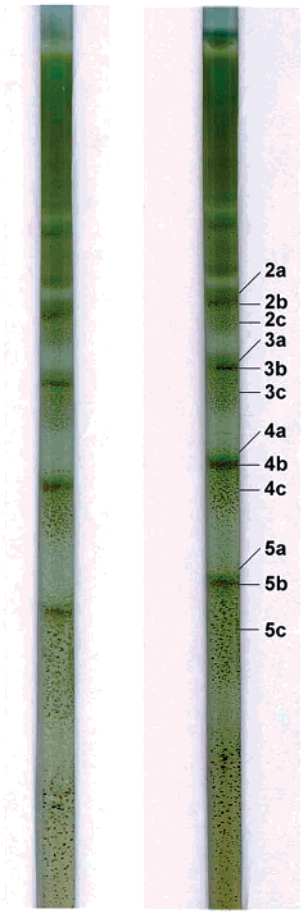

Figure 8. Two-precipitate pattern of cobalt oxinate and copper oxinate. $[Ox]_o = 0.010$ M, $[Co^{2+}]_o = 0.076$ M, $[Cu^{2+}]_o = 0.10$ M. Pattern age: 273 days. The precipitate content (in the two salts) of every zone is given in Table 2.

TABLE 2: Composition of the Various Bands in a Cobalt Oxinate/Copper Oxinate Liesegang Pattern Showing the Percent Weights of the Salts[a]

	% $Co(Ox)_2$	% $Cu(Ox)_2$
2a	74.6	25.4
2b	29.2	70.8
2c	68.7	31.3
3a	17.1	82.9
3b	36.0	64.0
3c	7.1	92.9
4a	16.0	84.0
4b	37.1	62.9
4c	3.0	97.0
5a	11.5	88.5
5b	45.3	54.7
5c	25.8	74.2

[a] The pattern is obtained by diffusion of a solution 0.10 M in Cu^{2+} and 0.076 M in Co^{2+} into a 0.010 M oxine gel. The band numbers correspond to the ones seen in Figure 8.

We now consider the cobalt oxinate/zinc oxinate pattern, which is shown in Figure 10. The initial concentrations of the reagents are given in Section 2.2 and in the captions of Figure 10 and Table 3. The contents of the various parts were analyzed by atomic absorption spectrophotometry. The Co^{2+}/Zn^{2+} proportions of a given part were converted to relative masses of cobalt oxinate and zinc oxinate precipitates. The mass percents are reported in Table 3. Interesting features are particularly noted in this case. Although the initial concentration of Zn^{2+} is larger than that of Co^{2+} (in the diffusing solution), the cobalt and zinc oxinate salts overlap, but with a gradually increasing dominance

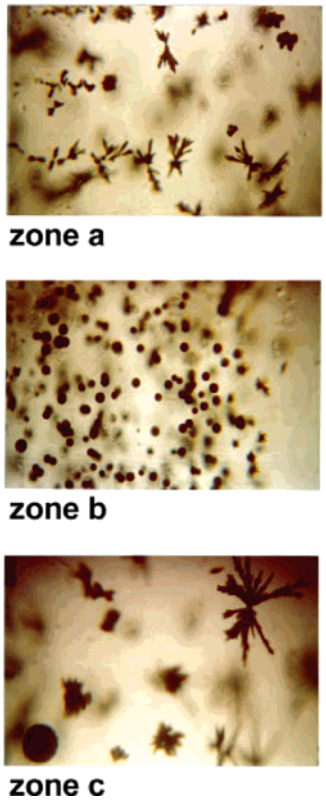

Figure 9. Photomicrographs of zones a, b, and c in a typical band of the $Co(Ox)_2/Cu(Ox)_2$ pattern shown in Figure 8. The particle size in zones a and c is larger than in the middle zone (b).

Figure 10. Two-precipitate pattern of cobalt oxinate and zinc oxinate. $[Ox]_o = 0.010$ M, $[Co^{2+}]_o = 0.076$ M, $[Zn^{2+}]_o = 0.15$ M. Pattern age: 239 days. The precipitate content (in the two salts) of every band is given in Table 3.

of the cobalt salt at long times (higher band numbers). This realization suggests that the topology of the pattern is determined by thermodynamic factors. A competition between the two salts could resemble the one between the silica polymorphs obtained in ref 43, governed by a free-energy scenario. Therein, the quartz polymorph dominates at long times. Various factors such as the solubility constants, the adsorption energy, and the interface curvature driven by mass transport through diffusion contribute to the stability of the dominant phase.

TABLE 3: Composition of the Various Bands in a Cobalt Oxinate/Zinc Oxinate Liesegang Pattern, Showing the Percent Weights of the Salts[a]

	% $Co(Ox)_2$	% $Zn(Ox)_2$
1	54.2	45.8
2	54.7	45.3
3	72.6	27.4
4	75.9	24.1
5	92.8	7.2
6	91.5	8.5
7	87.7	12.3
8	93.7	6.3

[a] The pattern is obtained by diffusion of a solution 0.15 M in Zn^{2+} and 0.076 M in Co^{2+} into a 0.010 M oxine gel. The band numbers correspond to the ones shown in Figure 10.

6. Conclusions

The main results of this study on single and two-salt metal oxinates may now be summarized as follows:

1. In cobalt oxinate Liesegang patterns with the same initial concentration difference, the average particle size increases while the number of bands and the number of particles (within a given band) decrease as the initial supersaturation increases.

2. The particle size distribution was measured over the constituent bands of the pattern. The pattern evolves toward fewer but larger particles as we go through the bands from top to bottom, as is observed upon time aging during an Ostwald ripening evolution.

3. A new counting and measuring algorithm based on the Watershed Segmentation method was developed, to allow the measurement of the particle size distribution by an image analysis technique.

4. Two-salt patterns of cobalt oxinate and copper oxinate displayed zonation within a single band, with each domain consisting of a scatter of particles of both precipitates.

5. Two-salt patterns of cobalt oxinate and zinc oxinate yielded an overlap of the two salts in dense band domains, with a gradually increasing dominance of the cobalt salt as we go toward the bottom bands (later times).

Acknowledgment. This work was supported by a University Research Board (URB) grant, American University of Beirut. We thank Noha Al-Kassem and Hasan Zayat for their trials on this system in the initial stages of the project.

References and Notes

(1) Liesegang, R. E. *Chemische Fernwirkung, Lieseg. Photograph. Arch.* **1896**, *37*, 305; continued in *37*, 331.

(2) Henisch, H. K. *Crystals in Gels and Liesegang Rings*; Cambridge University Press: Cambridge, 1988.

(3) Hedges, E. S.; Myers, J. E. *The Problem of Physico-Chemical Periodicity*; Longmans Green: London, 1926.

(4) Goldbeter, A. *Biochemical Oscillations and Cellular Rhythms*; Cambridge University Press: Cambridge, 1996.

(5) *Bacteria as Multicellular Organisms*; Shapiro, J. A., Dworkin, M., Eds.; Oxford University Press: New York, 1997.

(6) Kravchenko, V. V.; Medvinskii, A. B.; Reshetilov, A. N.; Ivanitskii, G. R. *Dokl. Akad. Nauk* **1999**, *364*, 114 and 687.

(7) Liesegang, R. E. *Geologische Diffusionen*; Steinkopff: Dresden, 1913; *Die Achate*; Steinkopf: Dresden-Leipsig, 1915.

(8) *Fractals and Dynamic Systems in Geoscience*; Kruhl, J. H., Ed.; Springer-Verlag: Berlin, 1994; see also references therein.
(9) Ortoleva, P. *Geochemical Self-Organization*; Oxford University Press: New York, 1994.
(10) Moxon, T. *Educ. Chem.* **2001**, *July issue*, 105.
(11) Sultan, R.; Ortoleva, P. *Physica D* **1993**, *63*, 202.
(12) Feinn, D.; Scalf, W.; Ortoleva, P.; Schmidt, S.; Wolff, M. *J. Chem. Phys.* **1978**, *69*, 27.
(13) Feeney, R.; Ortoleva, P.; Strickholm, P.; Schmidt, S.; Chadam, J. *J. Chem. Phys.* **1983**, *78*, 1293.
(14) Lovett, R.; Ortoleva, P.; Ross, J. *J. Chem. Phys.* **1978**, *69*, 947.
(15) Ostwald, Wi. *Z. Phys. Chem.* **1900**, *34*, 495.
(16) Ratke, L.; Vorhees, P. W. *Growth and Coarsening, Ostwald Ripening in Material Processing*; Springer: Berlin, 2002.
(17) Lifshitz, I. M.; Slyozov, V. V. *J. Phys. Chem. Solids* **1961**, *19*, 35.
(18) Walton, A. E. *The Formation and Properties of Precipitates*; Krieger: New York, 1979.
(19) Flicker, M.; Ross, J. *J. Chem. Phys.* **1974**, *60*, 3458.
(20) Panjarian, Sh.; Sultan, R. *Collec. Czech. Chem. Commun.* **2001**, *66*, 541.
(21) Kanniah, N.; Gnanam, F. D.; Ramasamy, P. *Proc. Indian Acad. Sci., Chem. Sci.* **1984**, *93*, 801.
(22) Kolthoff, I. M.; Sandell, E. B. *Textbook of Quantitative Inorganic Analysis*; The Macmillan Company: New York, 1958.
(23) Vogel, A. A. *A Textbook in Quantitative Inorganic Analysis*, 4th ed.; Longmann Scientific and Technical: London, 1978; p 423.
(24) *Handbook of Solvents*; Wypych, G., Ed.; W. Andrew and ChemTech Publishing: Toronto, 2001.
(25) Müller, S. C.; Kai, S.; Ross, J. *J. Phys. Chem.* **1982**, *86*, 4078.
(26) Müller, S. C.; Kai, S.; Ross, J. *J. Phys. Chem.* **1982**, *86*, 4294.
(27) Tai, C. Y.; Chien, W.-C.; Chen, P.-C. In *Encyclopedia of Surface and Colloid Science*; Hubbard, A. T., Ed.; Dekker Digital Publishers: 2002; pp 3903−3918.
(28) Boudreau, A. E. *Mineral. Petrol.* **1995**, *54*, 55.
(29) http://www.pace.edu/dyson/academics/chemistryplv/rahnidocs/che111/; Chapter 8 (power point presentation).
(30) Barata, P. A.; Serrano, M. L. *J. Cryst. Growth* **1998**, *194*, 109. Blumenthal, N. C.; Posner, A. S.; Holmes, J. M. *Mater. Res. Bull.* **1972**, *7*, 1181. Weintritt, D. J.; Cowan, J. C. *J. Petr. Technol.* **1967**, *19*, 1381.
(31) http://www.csudh.edu/oliver/che230/textbook/Grav03.htm; http://www.globetech.co.kr/english/main6_center.htm; http://web.odu.edu/webroot/instr/sci/ppleban.nsf/pages/321chap5.
(32) Pagliolico, S.; Marchisio, D.; Barresi, A. A. *J. Therm. Anal. Calorim.* **1999**, *56*, 1423.
(33) Chang, Y.-W.; Kim, W.-So; Kim, W.-Si. *Kor. J. Chem. Eng.* **1996**, *13*, 496.
(34) Judat, B.; Kind, M. http://www.aidic.it/ISIC15/isicwebpapers/140%20Judat.pdf.
(35) Hatakka, H.; Oinas, P.; Reunanen, J.; Palosaari, S. http://www.lut.fi/~hhatakka/docit/agglo.html.
(36) Sadek, S. M.Sc. Thesis, American University of Beirut, 1995.
(37) Kai, S.; Müller, S. C.; Ross, J. *J. Chem. Phys.* **1982**, *76*, 1392.
(38) Scharf, G.; Eulitz, J. *Metall.* **1975**, *29*, 358.
(39) Ostwald, Wi. *Lehrbuch der Allgemeinen Chemie*, 2. Aufl., Band II, 2. Teil: Verwandtschaftslehre, Engelmann, Leipzig, 1899; p 779.
(40) Prager, S. *J. Chem. Phys.* **1956**, *25*, 279.
(41) Becker, R.; Döring, W. *Ann. Phys.* **1935**, *24*, 719.
(42) Wattis, J. A. D. *J. Phys. A: Math. Gen.* **1999**, *32*, 8755.
(43) Ozkan, G.; Ortoleva, P. *J. Chem. Phys.* **2000**, *112*, 10510.
(44) Kai, S.; Müller, S. C.; Ross, J. *J. Phys. Chem.* **1983**, *87*, 806.
(45) Dee, G. T. *Phys. Rev. Lett.* **1986**, *57*, 275.
(46) Ballard, D. H. *J. Pattern Recognition* **1981**, *13*, 111. Guil, N.; Zapata, E. L. *J. Pattern Recognition* **1997**, *30*, 1729. Illingworth, J.; Kittler, J. *IEEE Trans. PAMI* **1987**, *9*, 1. Tsuji, S.; Matsumoto, F. *IEEE Trans. Comput. C* **1978**, *27*, 777.
(47) *Mathematical Morphology in Image Processing*; Dougherty, E., Ed.; Marcel Dekker: New York, 1992. Chen, C. H.; Pau, L. F.; Wang, P. S. P. *Handbook of Pattern Recognition and Computer Vision*; World Scientific: 1993. Meyer, F.; Beucher, S. *J. Vis. Comm. Im. Rep.* **1990**, *1*, 21.
(48) Gonzalez, R. C.; Woods, R. E. *Digital Image Processing*; Prentice-Hall: 2002.
(49) Russ, J. *The Image Processing Handbook*; CRC Press: 1998.
(50) Soille, P. *Morphological Image Analysis: Principles and Applications*; Springer-Verlag: Berlin & Heidelberg, 1999.
(51) Chacron, M.; L'Heureux, I. *Phys. Lett. A* **1999**, *263*, 70.
(52) Msharrafieh, M.; Al-Ghoul, M.; Sultan, R. in preparation for submission; for the model, see: Al-Ghoul, M.; Sultan R. *J. Phys. Chem. A* **2001**, *105*, 8053. Shreif, Z.; Al-Ghoul, M.; Sultan, R. *ChemPhysChem* **2002**, *3(7)*, 592.